Modeling lateral enlargement in dam breaches using slope stability analysis based on circular slip mode

Lin Wang [a], Zuyu Chen [b,*], Naixin Wang [b], Ping Sun [b], Shu Yu [b], Shouyi Li [a], Xiaohu Du [c]

[a] State Key Laboratory Base of Eco-hydraulic Engineering in Arid Area (Xi'an University of Technology), Institute of Water Resources and Hydropower Engineering, Xi'an University of Technology, 5, Jinhua, South Road, Xi'an, 710048, P. R. China
[b] State Key Laboratory of Simulation and Regulation of Water Cycle in River Basin, China Institute of Water Resources and Hydropower Research, 20 Chegongzhuang West Road, Beijing 100048, P. R. China
[c] China Renewable Energy Engineering Institute, 5 Liupukang South Road, Beijing 100120, P. R. China

ABSTRACT

Evaluation of breach flood of landslide or artificial dams is usually performed by combining the hydraulic modeling of the breach flow and geotechnical analysis of the breach channel stability. This paper is a continuation of the previous work, which mainly focused on the hydraulic aspects of a dam breach flood. Efforts have been made to improve the related slope stability analysis approach that traditionally adopts a simple wedge failure mode. The improvements includes a vertical cut at the slope toe due to soil erosion, an approach to determine the critical slip surface, the effective and total stress methods dealing with different dam materials, and a procedure to model the stepped failures of the breach bank due to continuous toe cutting. Using VBA programming, an Excel spreadsheet entitled DBS-IWHR has been developed to perform the stability analysis. This spreadsheet has been incorporated into another spreadsheet entitled DB-IWHR for the calculation of the flood hydrograph. The developed model has been tested by back analysis of the Yigong landslide dam breached at the Tibetan Plateau in China in 2000 with a flood peak of 94,013 m³/s. The calculated results of the final breach base level and the peak discharge are in good agreement with the field data. Further, the results are shown to be insensitive to the variations in the geotechnical parameters used in the model.

© 2016 Elsevier B.V. All rights reserved.

1. Introduction

For safety control, it is important to estimate the flood due to the breach of natural or artificial dams (ASCE/EWRI Task Committee 2011). For this type of estimation, a dam breach analytical model usually combines hydraulic and geological approaches. The flow discharge passing through the breach opening is usually determined by the broad crested weir flow formula. As the base of the breach is cut deep to a certain elevation, the banks on both sides of the channel may collapse, resulting in a wider channel. This is known as lateral enlargement. For this type of dam breach analysis, as a preliminary approach, the planar wedge failure mode is usually used in the slope stability analysis (e.g., Fread, 1988). The process of 'cut and collapse' cycle continues until the reservoir water is depleted.

In this study, the authors' research group had the opportunity to examine the documented field monitored information of the draining process of the Tangjiashan barrier lake. Based on an in-depth back analysis of the monitored data, Chen et al. (2015) proposed improvements to the existing dam breach analytical methods. These improvements enable the dam breach flood analysis to be less sensitive to the input parameters. It can also be performed using a simple coded Excel 2013 spreadsheet, namely DB-IWHR. Due to the limitation of space, the earlier paper (Chen et al., 2015) mainly focused on the hydraulic aspects of the improved method. The present paper provides the details on the modeling of lateral enlargement of a breach during a dam breach process.

Since the slope stability analysis contains tedious procedures (e.g., modeling of a vertical toe cutting and stepped collapsing, searching for the critical slip surface and applying a total stress analysis method), a spreadsheet for computing the lateral enlargement process, namely, the DBS-IWHR, in conjunction with the DB-IWHR, has been developed. This spreadsheet enables the practitioners to carry out their routine stability analyses on predicting the dam breach flood. It is available for downloading at the website: http://www.geoeng.iwhr.com/geoeng/download.htm.

The developed method is applied in the back analysis of a gigantic landslide dam breach that occurred in Yigong in the Tibet Plateau in 2000 with a flood peak of 94,013 m³/s.

* Corresponding author.
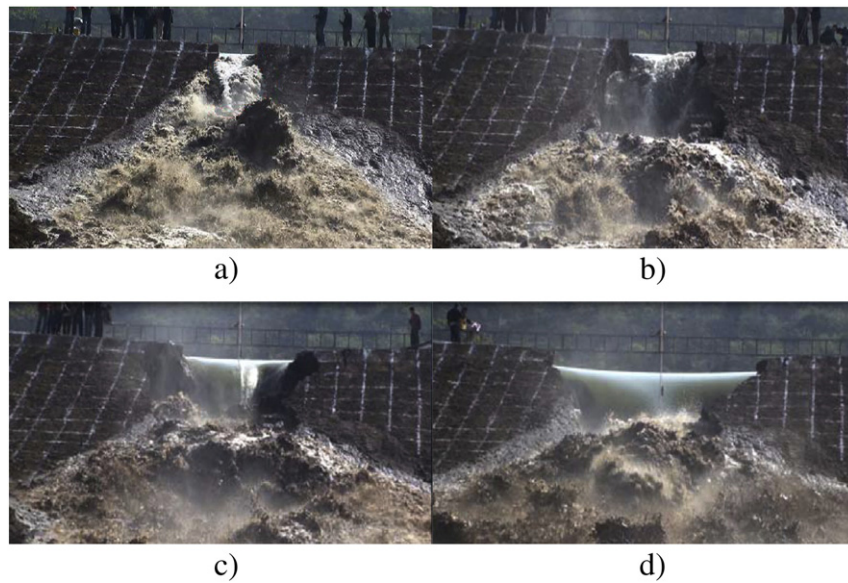 E-mail address: chenzuyu@cashq.ac.cn (Z. Chen).

Fig. 1. The enlargement process of a model dam in different elapsed times: (a) 210s; (b) 360s; (c) 480s; (d) 520s (Zhang et al., 2009, courtesy by Shengshui Chen).

2. Modeling lateral enlargement

2.1. Lateral enlargement of breached bank due to slope instability

The continuous enlargement of a dam breach opening is a phenomenon commonly observed in the field and laboratories. For example, Liu et al. (2010) reported that during the breach of the landslide dam at the Tangjiashan barrier lake, the width of the channel was enlarged from 7 m to 150 m. Fig. 1 shows the enlargement process during the breaching process of a 9.7 m high model dam (Zhang et al., 2009). Further, for the same model dam, Fig. 2 catches the instant of 360 s, shown as Fig. 1(b) in the previous pictures, when a slump of soil fell down, the red dotted lines clearly show the landslide process of the dam breach.

2.2. Discussion on previous work

In most of the existing dam breach analytical methods, the lateral enlargement of the channel is modeled using slope stability analysis methods. In these methods, a planar wedge failure mode is used in which the slip surface is assumed to be a straight line (Fread, 1988; Osman and Thorne, 1988; Singh and Scarlatos, 1988; Peviani, 1999; Mohamed, 2002; Zhu, 2006; D'Eliso, 2007; Huang, 2008; Wang et al., 2008; Morris et al., 2009b; Chang and Zhang, 2010; Viero et al., 2013; Wu, 2013; Dou et al., 2014; Peng et al., 2014). The necessary analytical details that should be considered include: (1) a vertical cut at the slope toe, (2) the approach to determining the critical slip surface, (3) appropriate consideration of the pore water pressure in the failed slope, and (4) the procedure to model the stepped failures of the breach bank due to continuous toe cutting. The method proposed by Osman and Thorne (1988) appears to have considered most of the aforementioned details, especially the vertical cut at the toe, and has therefore encountered wide applications (Huang, 2008; Wang et al., 2008; Morris et al., 2009a, b).

Apart from these aspects, it should also be noted that the geotechnical profession has a long history of assessing the stability of a slope by circular or more generalized shaped failure surfaces (Bishop, 1955; Morgenstern and Price, 1965). It is also noted that the pore water pressure or phreatic line in the dam body is invariably ignored in all the existing methods.
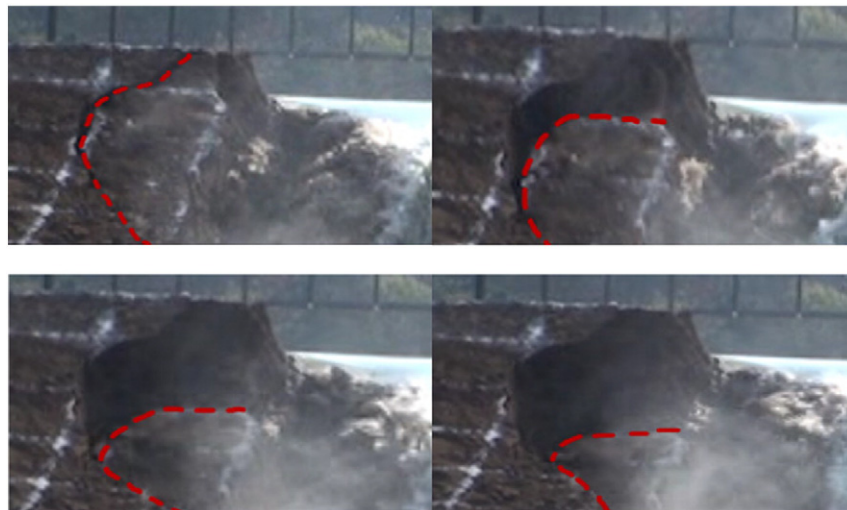

Fig. 2. The detailed landslide process happened in the right bank of the breach at 360 s shown in Fig. 1(b) (Zhang et al., 2009, courtesy by Shengshui Chen).
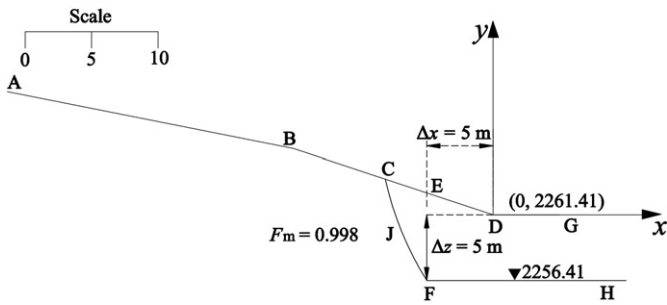
Fig. 3. The first round bank collapse analysis for Yigong landslide dam.

Perhaps this wedge failure mode is used because it has an easy, straightforward formulation for determining the lateral enlargement. It can be conveniently incorporated into a dam breach analysis program which contains many iterative procedures. Use of spreadsheets may be an alternative that allows the application of more rigorous methods without too much effort of additional manual undertakings. The authors' previous work on DB-IWHR (Chen et al., 2015) is such an example in which the dam breach hydrograph can be calculated and displayed. Similarly, the geotechnical computation work related to the lateral enlargement can also be performed in another spreadsheet.

3. The improved method

3.1. Performing slope stability analysis using a spreadsheet

Use of a spreadsheet to carry out slope stability analysis can be traced back to Low et al. (1998). They used the closed-form equations for satisfying the force and moment equilibrium conditions proposed by Chen and Morgenstern (1983), thereby allowing easy manipulation in a spreadsheet. However, the information regarding weight, strength and geometry of each slice of a slope still requires manual calculation and input. Chen et al. (2008) therefore developed an improved version in which the geometrical information of a slope is automatically acquired from an AutoCad drawing with the LISP language. The information is then transferred to the spreadsheet with the aid of VBA programming provided by Excel. With the improved version, the factor of safety for a slope can then be calculated by a user-friendly, transparent spreadsheet without the need of any manual calculations.

3.2. DBS-IWHR Spreadsheet

DBS-IWHR is developed as an extension to the previous work by Chen et al. (2008) for the particular purpose of modeling the lateral enlargement of a dam breach. Its main structure and functions are given in Appendix A.
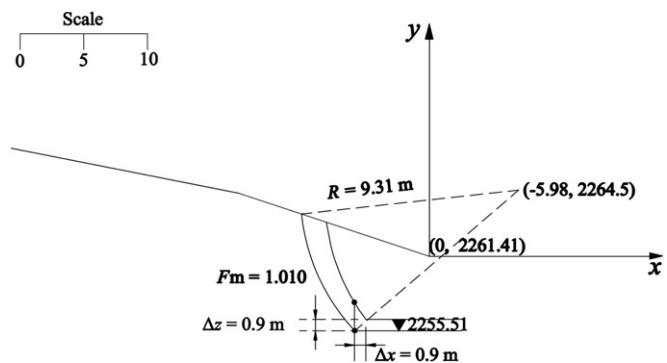

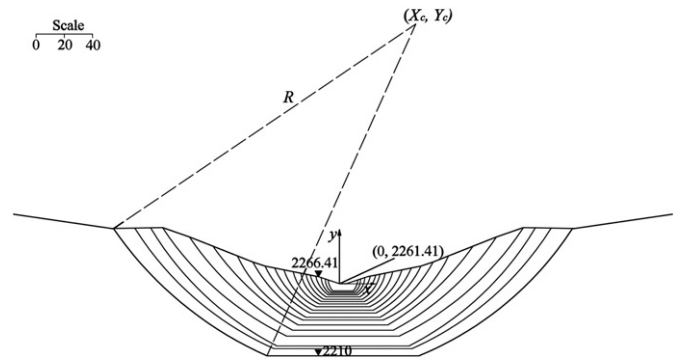Fig. 4. The second round bank collapse analysis for Yigong landslide dam.

Fig. 5. Cross-sections of the 19 bank collapses for Yigong landslide dam.

3.2.1. Stability analysis for a circular slip surface

In DBS-IWHR, Bishop's simplified method (1960) is used to calculate the factor of safety of a circular slip surface, as follows:

$$F = \frac{\sum_{n=1}^{N}\left[\Delta W(1-r_u)\tan\phi' + c'\Delta x\right]/\left[\cos\alpha(1+\tan\alpha\tan\phi'/F)\right]}{\sum_{n=1}^{N}\Delta W\sin\alpha} \quad (1)$$

where, F is the factor of safety, α is angle of inclination at the base of a slice, ΔW is the weight at the base of a slice, Δx is the width at the base of a slice, c' and ϕ' are effective cohesion and friction angle, respectively, at the base of the slice. r_u is the pore pressure ratio defined as:

$$r_u = \frac{u\Delta x}{\Delta W} = \frac{u}{\gamma_{avg}h'} \quad (2)$$

where, u is the pore pressure at the base of a slice, h' is the height of the slice, and γ_{avg} is the unit weight of the slice.

3.2.2. Automated search for the critical slip surface

Although the minimum factor of safety can be determined using various optimization methods (Duncan, 1996), DBS-IWHR uses the simplest two-step grid search method. Details are given in Appendix A.

As shown in Fig. 3, the original slope profile is represented by ABCEDG. When the toe, as denoted by D, is cut vertically by Δz from elevation 2261.41 m to 2256.41 m, and is also eroded horizontally towards the slope with the same magnitude of 5 m to the new position F, the factor of safety F_m of the slope with the surface contour ABCEFH reduces to 0.998. A landslide is believed to occur, resulting in the resultant surface contour represented by ABCJFH.

3.2.3. Modeling the stepped failure process

The second sudden enlargement is initiated by the continuous toe cutting that can be evaluated using the same procedure as the first. However, the slope analysis is then performed on the resultant dam
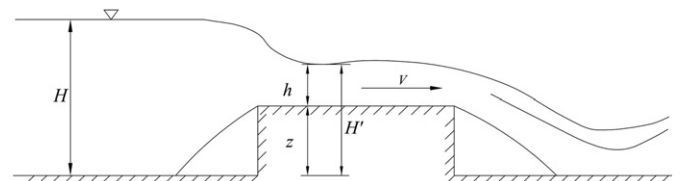

Fig. 6. Hydraulic relations at entrance of channel.

Table 1
Numerical method.

Step	Symbol	Parameters	Equation
0	ΔV	Input of the integration step in terms of V	
1	$\overline{V}$	Average velocity	$\overline{V} = V_o + \Delta V/2$
2	s	$s = \Delta z - \Delta H$	$s = 2(\frac{m\overline{V}}{C})^2 - 2(H_o - z_o)$
3	h	Depth of the flow	$h = m(H_0 - z_0 + 0.5s)$
4	$\overline{\tau}$	Shear stress	$\overline{\tau} = \gamma n^2 V^2 / h^{1/3}$
5	Δz	Decrease in channel bed elevation	$\Delta z = \frac{s}{1-L}$ where $L = \frac{m\overline{V}B_o(H_o - z_o + 0.5s) - q}{\Phi(\overline{\tau})\frac{\Delta W}{\Delta H}}$
6	z	Channel bed elevation	$z = z_o - \Delta z$
7	H	Reservoir water level	$H = H_o + s - \Delta z$
8	Δt	Time interval at this integration step with the given ΔV	$\Delta t = \frac{\Delta z}{\Phi(\overline{\tau})}$
9	Q	Discharge through the channel	$Q = CB(H - z)^{3/2}$

Note: In Step 4, $\overline{\tau}$ is the shear stress, γ is the density of water, n is the roughness coefficient (0.025 m$^{-1/3}\cdot$s in this case), and h is the flow depth.

body created in the first slip. DBS-IWHR has a function of transferring the slope contour ABCJFH obtained from the first slip to the second slip and refreshing it so that the second stepped sudden enlargement process can be implemented almost automatically. For the second

enlargement, a new toe cutting depth Δz of 0.9 m with F_m value of 1.010 is obtained, as shown in Fig. 4.

For the Yigong case, which will be illustrated in detail in Section 4, a total of 19 steps were simulated to examine the bank collapse process from elevation 2256.41 m to 2210.00 m with cross-sections as shown in Fig. 5. Since the main purpose of this work is to compare the calculated flood with field measurement which stopped at 19:00 on June 11 when the reservoir water level was 2209.81 m, no more efforts were made for modeling any further failures.

3.2.4. The effective versus total stress analysis

During the process of dam breach, the water level in the breached channel drops rapidly. As such, the stability of the slope should be analyzed in an undrained condition. This is similar to the rapid drawdown of reservoir water behind an embankment dam (Lowe and Karafiath, 1960; Sherard et al., 1963; Johnson, 1974).

DBS-IWHR considers two cases that are commonly encountered in dam breach analysis.

The first case is where the dam body is dry and free of groundwater. This case relates to a rockfill or landslide dam. In the analysis, Eq. (1) is used with the effective stress method, in which the input $r_u = 0$, or some other value as specified by the user.
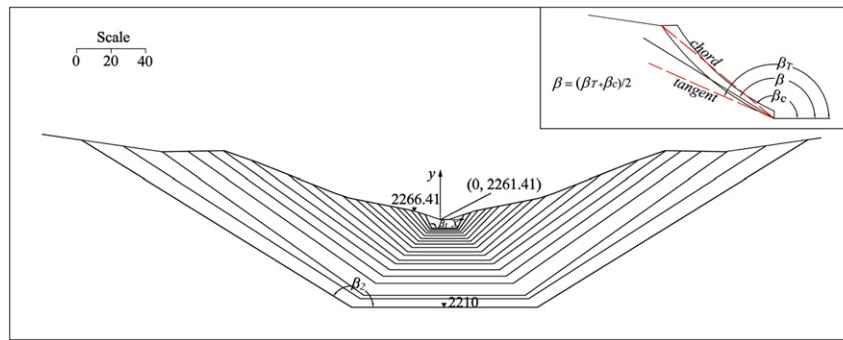

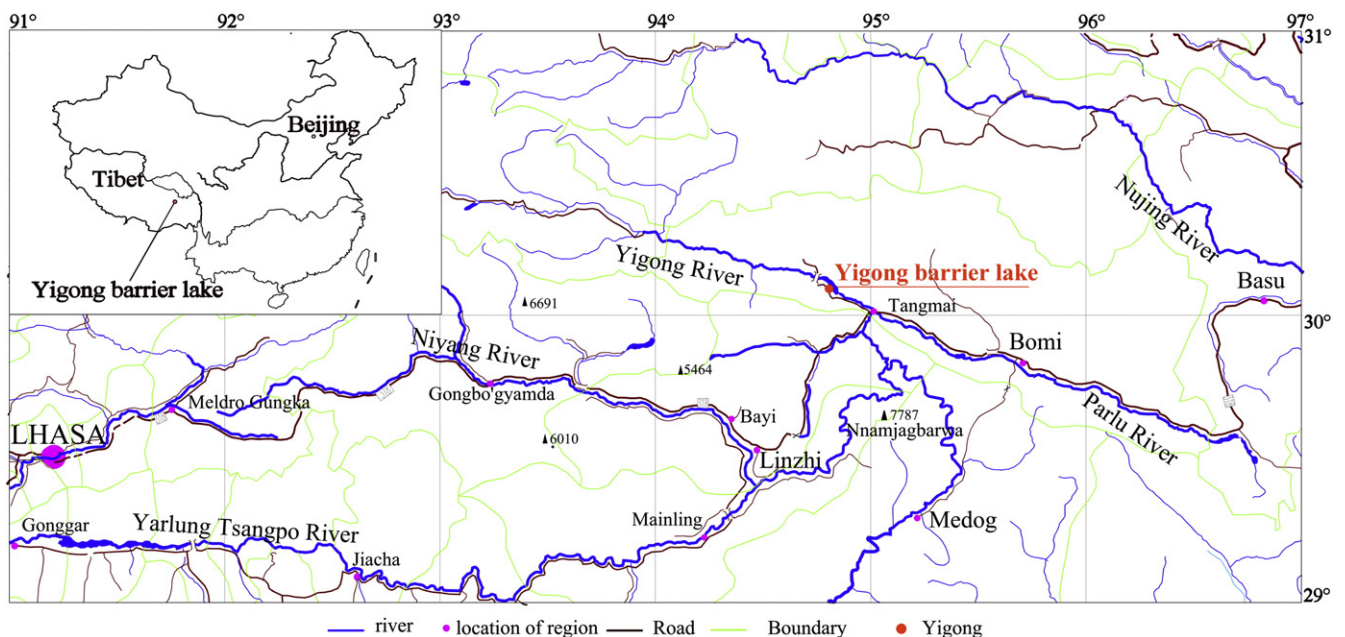**Fig. 7.** Equivalent simplification of lateral enlargement process.

Fig. 8. Location of Yigong barrier lake.

Fig. 9. Yigong barrier lake.

The second case is where the dam body is fully saturated and a phreatic line exists within the dam body before it fails. This case relates to a dam made of thick impervious material such as clay and tailings.

Both effective stress (Bishop and Morgenstern, 1960; Morgenstern and Price, 1965) and total stress (Lowe and Karafiath, 1960; Sherard et al., 1963; Johnson, 1974) methods have been used in the analysis.

Since it is difficult to determine the pore pressure coefficients A and B (Skempton, 1954), it is normally difficult to use the effective stress method in a dam breach analysis. As such, the total stress method has been widely used with the consolidated undrained strength parameters. In fact, in the manual by the US Army Corps of Engineers' (1970), there is a well-documented computing procedure. There are three steps in this procedure, which are associated with cases before and after drawdown and an approach of using the composite strength envelope (Johnson, 1974). DBS-IWHR uses a simplified version of the procedure, as follows:

1) Determine the effective stress σ_c' at the base of a slice prior to rapid drawdown, as follows:

$$\sigma_c' = \frac{\Delta W'}{\Delta x} \cos\alpha \tag{3}$$

where, $\Delta W'$ is the effective weight of the slice, which is determined based on unsaturated and buoyant weights for the parts above and below the phreatic line, respectively.

2) Determine the undrained strength S_u as follows

$$c' = S_u = c_{cu} + \sigma_c' \tan\phi_{cu} \tag{4}$$

where, c_{cu} and ϕ_{cu} are consolidated undrained shear strength parameters.

3) With the condition

$$\phi' = 0 \tag{5}$$

Eq. (1) becomes

$$F = \frac{\sum\limits_{n=1}^{N} S_u \Delta x \sec\alpha}{\sum\limits_{n=1}^{N} \Delta W \sin\alpha} \tag{6}$$

In the analysis, the phreatic line is considered unchanged during the breach.

3.3. Incorporating DBS-IWHR into DB-IWHR

The dam breach flood analytical model in DB-IWHR has been developed by equating the discharge through the breach, which has been modeled as a broad crested weir, to the loss of water storage in the reservoir in a unit time, as follows:

$$CB(H-z)^{3/2} = \frac{\Delta W}{\Delta H}\frac{\Delta H}{\Delta t} + q \tag{7}$$

where, C is the discharge coefficient, B is the width of the weir, H is the elevation of the water level and z is the elevation of the base of the breach, q is the inflow to the reservoir, W is water storage capacity in the reservoir, which is considered a function of water level H, and t is time. The physical dimensions in Eq. (7) are shown in Fig. 6 (Chen et al., 2015).

Further, the relationship between soil erosion rate $\dot{z}$ and shear stress $\overline{\tau}$ is described, as follows:

$$\dot{z} = \frac{\Delta z}{\Delta t} = \Phi(\overline{\tau}) \tag{8}$$

where, $\dot{z}$ is erosion rate in 10^{-3} mm/s, $\overline{\tau}$ is in Pa, and time t is in seconds.

DB-IWHR uses the coefficient m, which is defined as the water head drop ratio at the channel entrance, to determine the flow depth h.

$$m = \frac{h}{H-z} \tag{9}$$

Normally, m ranges from 0.4 to 0.8. In any case, it has been found that this coefficient does not affect the final solution of the peak flow appreciably (Chen, et al., 2015).

DB-IWHR has incorporated a number of soil erosion functions $\Phi(\overline{\tau})$, such as Meyer-Peter and Müller (1948), Brown (1950), Einstein

Table 2
Main characteristics of landslide slope, dam and barrier lake.

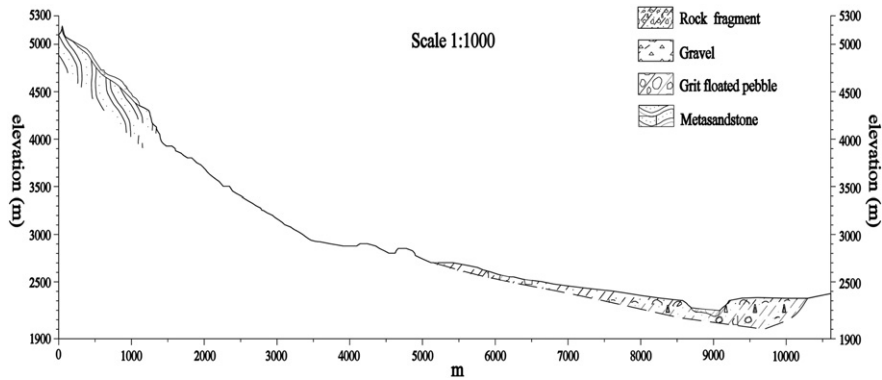| Item	Parameters	Magnitude
Landslide slope	Elevation of top of source rock mass	5520 m
	Horizontal distance	10,000 m
	Vertical height	3330 m
	Volume of source rock mass	0.3×10^9 m³
	Elevation of distal limit of debris	2186.41 m
Landslide dam	Volume of the landslide deposit	0.38×10^9 m³
	Elevations of crest/toe, measured at the lowest crest surface of the mid deposit	2266.41/2186.41 m
	Maximum/minimum dam height	100m/60 m
	Maximum/minimum bottom width (parallel to Yigong river flow)	2500/2200 m
Barrier lake	Highest water level	2267.06 m
	Potential storage of water	2.38×10^9 m³
	Potential area of the lake water surface	50.4 km²
	Elevation of the original river bed	2186.41 m

Fig. 10. Geological profile of the Yigong barrier lake.

(1950), and Engelund and Hansen (1967). In addition, it has also incorporated the hyperbolic model proposed by Chen et al. (2015). In this model, there is an asymptote $1/b$ representing the maximum possible erosion ratio and a parameter $1/a$ denoting the tangent of this curve at the incipient stress. These two parameters have sound physical meanings. As such, it can prevent unreasonable inflation of the calculated erosion at high velocity flow, which is normally encountered in a dam breach analysis. The calculated flood peak is less sensitive to the input parameters.

In solving the governing equations Eqs. (7) and (8), DB-IWHR uses a new approach that starts with the incipient velocity V_0 with an interval ΔV. This allows a straight forward calculation for all of the variables in Eqs. (7) and (8), without the need of any numerical iteration. Since the formulations and procedures have been fully explained in Chen et al. (2015), they are briefly summarized in Table 1. For s and L in Step 2 of the table, it has been found that they approach zero when the flow velocity V reaches its maximum. When the velocity passes its maximum, a negative velocity increment is used in the model. The calculation stops when V is decreased to the incipient velocity V_0.

As shown in Fig. 5, the information on the stepped failures becomes the input to DB-IWHR. However, if the details of the 19 steps of failure are input into DB-IWHR, it becomes too tedious for a dam breach analysis. On the other hand, there is not much loss in accuracy if the information of the intermediate steps is approximated using linear interpolation. Further, it requires more computation effort to determine the flow surface width. By remaining the original approach for circular channel sides based on Chen et al. (2015), the new version of DB-IWHR adds an option that simplifies the circular sided breached channel by a series of trapezoidal cross-sections. The inclination of the straight line channel side β is taken to be the average value of the inclinations of the chord and the tangent of the circle at the toe, as illustrated in Fig. 7. It has been found that the simplifications bring a great deal of convenience with only limited loss of computational accuracy. For example, the calculated flood peaks by the old and new versions of DB-IWHR for the Tangjiashan case reported by Chen et al. (2105) are 7610.0 m³/s and 7571.6 m³/s, respectively. However, it needs to be emphasized that either the circular or the simplified trapezoidal cross-sections may be utilized at the Users' discretion.

4. Back analysis of Yigong barrier lake

4.1. Basic information

4.1.1. General description

On April 9, 2000, a giant landslide occurred at Bomi County in Tibet Plateau and destroyed the existing Yigong Lake. Fig. 8 shows the location of the Yigong barrier lake. Fig. 9 shows a view of the Yigong barrier lake. It included a 3330 m high failed slope and a total of 0.3×10^9 m³ debris flowed into the Yigong River. As a consequence, the debris blocked the river and created a barrier lake with a potential total water storage of 2.38×10^9 m³. Table 2 contains the main characteristics of the landslide slope, dam and barrier lake. On June 10, 2000, the impounding water of the reservoir overtopped the landslide dam and created a huge flood.

4.1.2. Geological and morphological information

The geology and morphology of the landslide have been documented in many publications (Yin, 2000; Ren et al., 2001; Lu et al., 2003; Shang et al., 2003; Wen et al., 2004; Huang, 2012; Xu et al., 2012; Yin
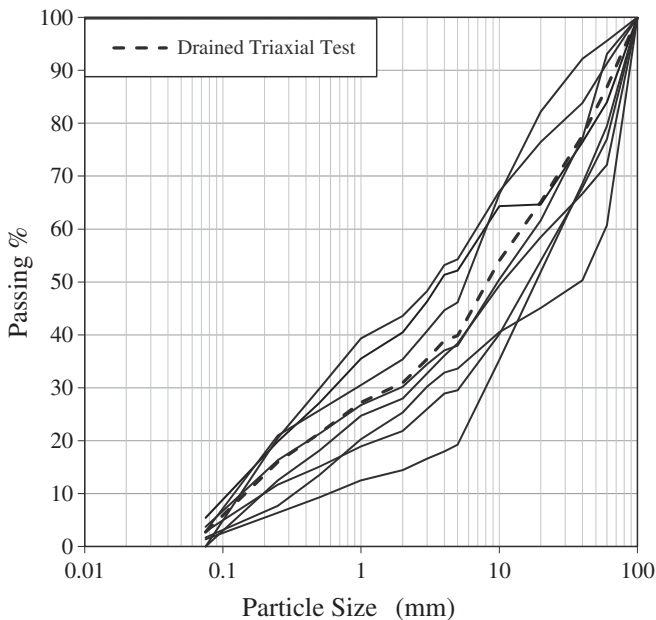

Fig. 11. Gain size distributions of Yigong landslide dam material.

Table 3
Drained triaxial test results.

Item	Dry density	d_{50}	c'	ϕ'
	g/cm³	mm	kPa	°
Unit	1.845	8	13	37
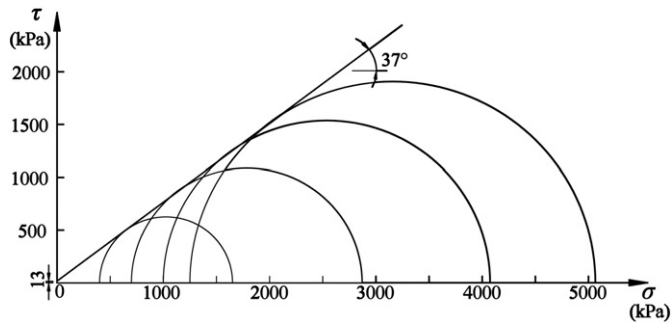
Fig. 12. The Mohr stress circle of the drained triaxial test.

Fig. 14. Measured reservoir water level versus time.

and Xing, 2012; Zhang and Yin, 2013; Zhou et al., 2015). Due to the difficulties in approaching this remote region, no topographical survey was performed during the emergency action period. In 2014, a field survey was performed. Fig. 10 shows a cross-section along the dam axis from which the width of the breach at the bottom of the residual dam body may be assumed to be around 430 m.

The authors held a field reconnaissance in 2014 and brought some debris material of the dam back to the laboratory. Fig. 11 gives the grain size distribution of the nine specimens tested. A drained triaxial test with the gradation curve shown as dashed lines in Fig. 11 was performed by assigning the geotechnical properties given in Table 3 and Fig. 12.

4.1.3. Hydrological information

There is only limited published information on the hydrological features of the dam breach. Delaney and Evans (2015) commented that the reported estimates of the peak breach discharge within 20 km of the breach are not well constrained. According to them, Shang et al. (2003), Zhu et al. (2003), and Xu et al. (2012) reported an estimated flood peak ranging between 120,000 m^3/s and 126,400 m^3/s and a total outburst volume of reservoir water of 3.0×10^9 m^3. However, based on satellite images, Delaney and Evans (2015) made an independent estimate of the flood peak, which was 61,461 m^3/s. This study uses the relevant information based on a recent publication by Liu et al. (2015) who presented the field measured hydrological data during the breach as documented in an official report by Office of Flood Control and Drought Relief Headquarter P.R.C. and nine other governmental and provincial authorities in 2005.

Liu et al. (2015) documented that right after the landslide dam was triggered, a field survey was performed which produced a relationship between the water storage and the elevation of the barrier lake, as shown in Fig. 13. Two hydrological gauging stations were established,
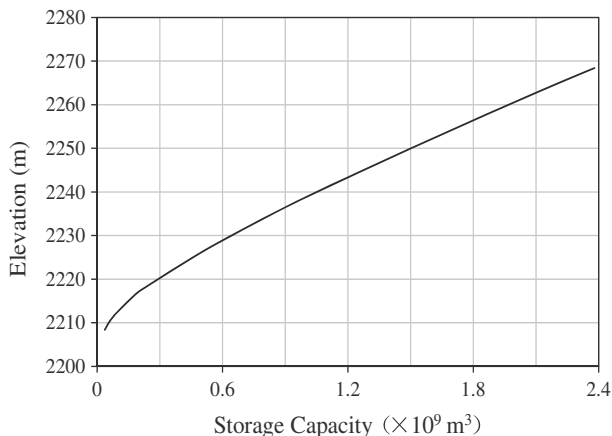
one at the upper reach of the reservoir at Gongde for runoff measurement, and the other at Chachang near the dam for measurement of the reservoir water level. Fig. 14 shows a complete record of the reservoir water level variations during the dam breach. The water storage-elevation relationship is shown in Fig. 13. Based on the loss of reservoir water per unit time a hydrograph of the dam breach flood was deduced, which is shown in Fig. 15. It can be observed that the dam breach started at 19:50 on June 10, when the water level in the reservoir started to decline. At 2:00 on June 11, the discharge reached its maximum of 94,013 m^3/s. After 19:00 on June 11, the water level in the reservoir was practically constant, which is an indication that the breaching process had ended. Hence, the entire breaching process lasted for about 24 h and the total volume of water released from the reservoir was 2.11×10^9 m^3. Fig. 16 shows a view of the drainage taking place in the Yigong barrier lake.

4.2. Dam breach flood analysis

Table 4 contains the inputs to DB-IWHR for the dam breach flood analysis. Fig. 17 shows the variations of the calculated hydrograph and the reservoir water level with time. Table 5 summarizes the calculated width B, the peak discharge Q_m, and volume of water released V_r. The calculated flood peak is 106,061 m^3 /s, as compared to 94,013 m^3/s derived from the field data.

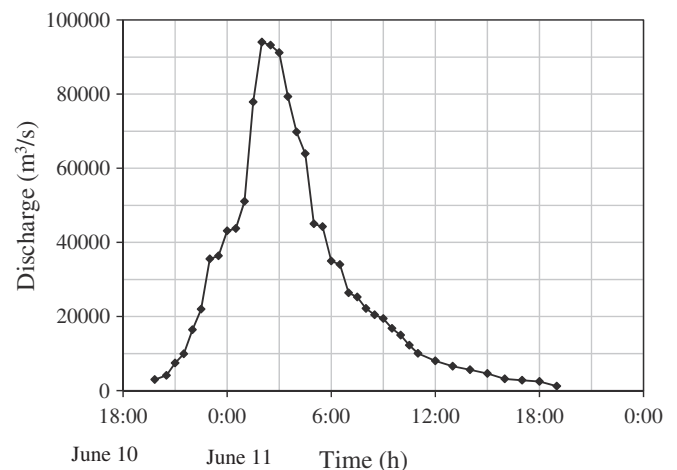**Fig. 13.** Relationship between water storage and elevation of the barrier lake.

Fig. 15. Measured dam breach flood (from 19:50 on June 10 to 19:00 on June 11).
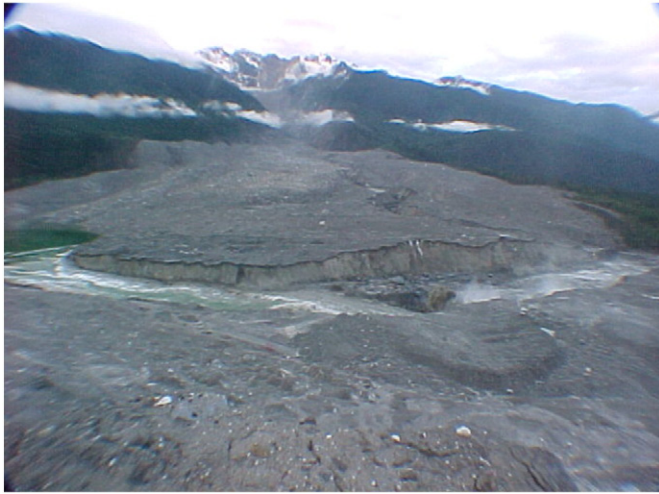
Fig. 16. Draining of the Yigong barrier lake.

4.2.1. Sensitivity studies

In view of the uncertainties in input parameters in the dam breach analysis, sensitivity study is normally an important part of dam breach analysis, as was done by Chen et al. (2015). However, this paper only investigates the uncertainties involved in lateral enlargement modeling in which the soil shear strength parameters have a direct effect on the calculated results.

The sensitivity study has used two sets of shear strength parameters as denoted by BA-upper and BA-lower in Table 5. Their values represent the probable upper and lower bound values. The calculated modes of stepped failures are shown in Fig. 18. The calculated results are presented in conjunction with those of the back analysis in Table 5. It can be found that the flood peak deviates in a small range within the reasonable range of input for shear strength parameters.

5. Conclusions

A dam breach flood analysis normally consists of two procedures:

(1) Modeling the hydraulic process based on the water balance between the released reservoir water and the outflow through the breached channel under the condition of a changing eroded channel.
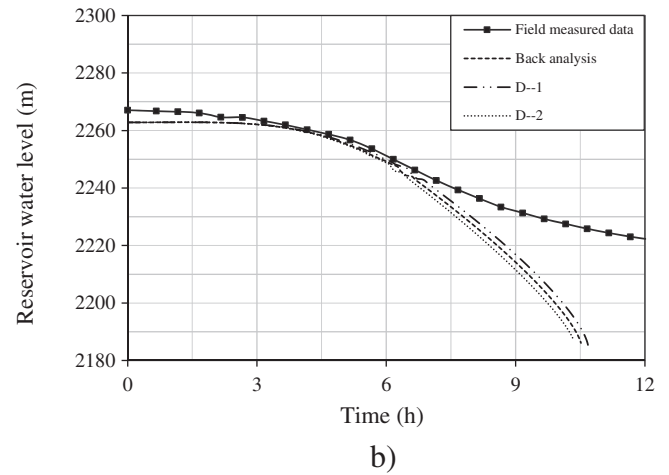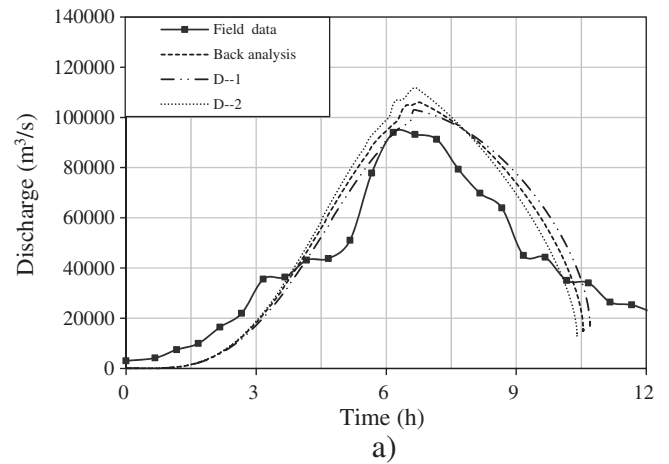
Table 4
Input parameters for back analysis case.

Item	Parameters	Values	Notes
Natural inflow	q	859 m^3/s	
Initial breach width	B_o	5 m	Determined based on the draining channel geometry and a flow height
Broad crested weir	C	1.35	Parameters involved in Eq. (7)
	m	0.8	Parameters involved in Eq. (9)
Reservoir water storage	p_1	0.31	The relationship between water storage and water level for Eq. (7) can be found in Fig. 14 and is approximated by $W = [p_1(H-H_r)^2 + p_2(H-H_r) + p_3] \times 10^6$ in m^3
	p_2	16.28	
	p_3	−121.78	
	Hr	2210 m	
Erosion rate	V_o	2 m/s	Parameters involved in Eqs. (7), (8) and Table 1
	a	0.3	
	b	0.00038	
Lateral enlargement	β_1	119°	Parameters involved in Fig. 7
	β_2	145°	
	Z_o	2261.41 m	
	Z_{end}	2210 m	

Note: Hr = elevation of dead water, V_0 = the incipient velocity, $1/b$ = the maximum possible erosion ratio, $1/a$ = the tangent of this curve at the incipient stress, β = the inclination of the straight line channel side, Z_o = incipient elevation of channel bed, Z_{end} = elevation ending.

a)

b)

Fig. 17. Comparison of calculated results with field data: (a) flow discharge; (b) reservoir water level.

(2) Finding the lateral enlargement process using stability analysis of the channel bank based on the conventional approaches in geotechnical engineering.

This paper presents details of the proposed analytical method for determining the lateral enlargement process which includes:

(1) Finding the factor of safety for a specific circular slip surface F.
(2) Among a variety of possible slip surfaces, determining the critical one associated with the minimum factor of safety F_m.
(3) Determining the critical depth of toe cutting associated with $F_m = 1$.
(4) Modeling the stepped bank failures due to the continuous erosion of the slope toe.

Table 5
Summaries of characteristic parameters for sensitivity studies.

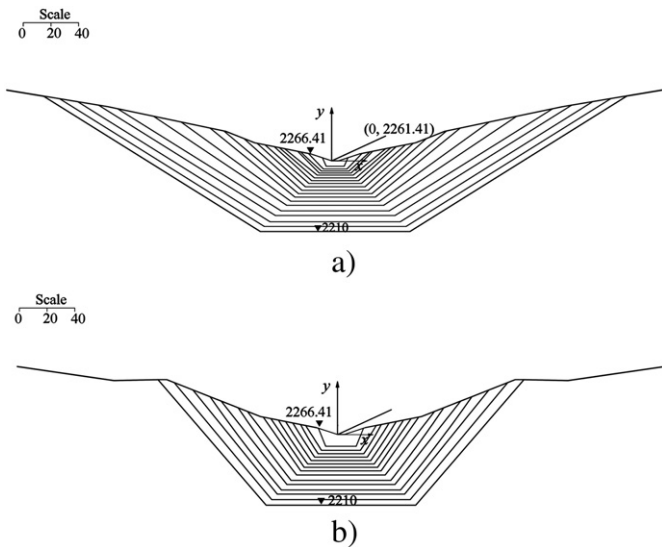| Case	Drained triaxial test		Flood peak		Breached channel	
	c'	φ'	t_m	Q_m	B	V_r
	kPa	°	hour	m^3/s	m	Total volume of released water ($\times 10^9$ m^3)
Field data			6.17	94,013.00	430.00	2.1073
Back analysis (BA)	13	37	6.77	106,061.67	424.64	1.9756
BA-upper	16	45	6.66	103,033.29	383.82	1.9789
BA-lower	10	30	6.69	111,754.10	473.09	1.9730

Fig. 18. Details of the cross-sections of the stepped lateral enlargement: (a) Ba-lower $c' = 10$ kPa, $\phi' = 30°$; (b) Ba-upper $c' = 16$ kPa, $\phi' = 45°$.

This research confirmed that the above 4-step computations on lateral enlargement can be automatically conducted by an Excel spreadsheet with the VBA programming with very little manual calculations. It can greatly facilitate the field engineers' work when a dam breach is impending. The spreadsheets are transparent and self-explanatory, easy for practitioners to understand and check, and allow for secondary development through the web.

The applicability of the proposed method has been further demonstrated by the back analysis of the breaching process of the Yigong barrier lake which has a flood peak of 94,013 m³/s. The calculated results show reasonable agreements with the field data, when the input properties of the material parameters are within a reasonable range known from experience and laboratory tests. In any case, the shear strength parameters have little effect on the calculated flood.
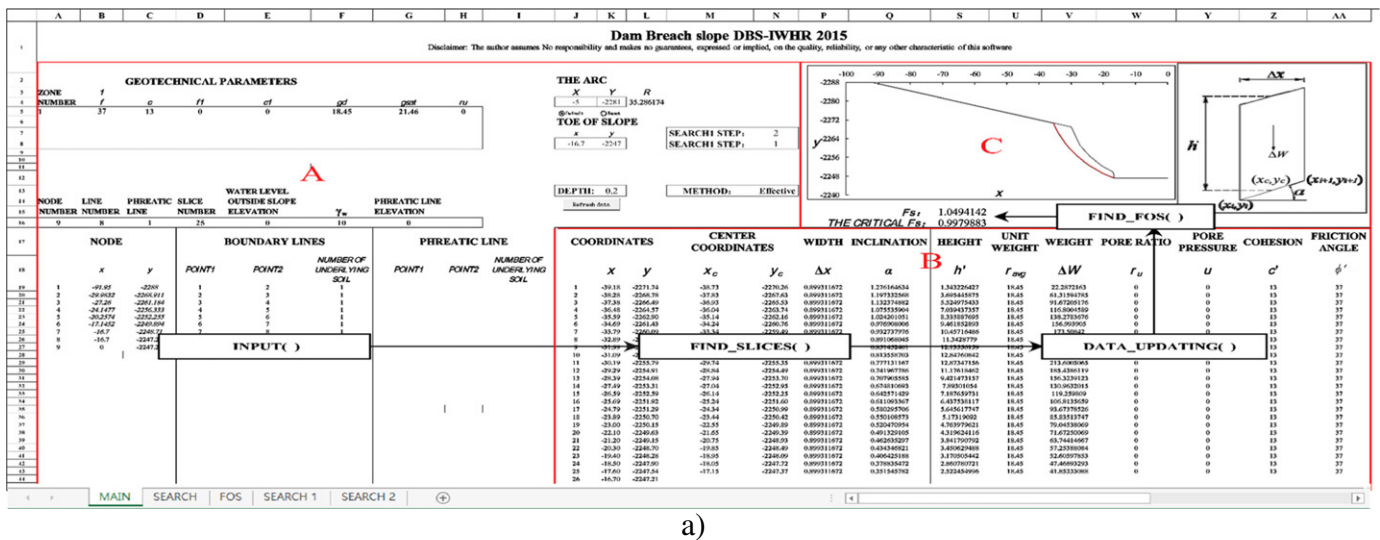
Acknowledgments

Appendix A. Structure and functions of DBS-IWHR Spreadsheet

A.1 Layout

Fig. A.1(a) shows the main structure of worksheet MAIN of DBS-IWHR which is coded in Excel. It comprises three zones:

Fig. A.1. Worksheets and flow charts: (a) Worksheet MAIN; (b) Subroutine FIND_SLICES; (c) Subroutine DATA_UPDATING.

Zone A is located at the upper left corner. It contains all the inputs, such as the slope geometry, material property and the initial circular slip surface to be investigated. The details are contained in Chen et al. (2008).

Zone B is located at the lower, right part of the sheet. It contains the information of the details of slices, such as their weight, strength, pore pressure ratio and so on.

Zone C is located at the upper right corner. It displays the calculated factor of safety and the graphic illustrations of the circle.

In addition to MAIN, a series of individual worksheets offer additional details that are related to the calculation, as may be seen in Fig. A.1(a) at the lowest part of the spreadsheet. They are: SEARCH, FOS, SEARCH 1, and SEARCH 2, which will be illustrated in the subsequent sections.

A.2. Calculation of factor of safety

Fig. A.1(a) shows the main flow chart of the calculation which contains the following steps:

Step 1: Subroutine INPUT initializes the input information contained in Zone A.

Step 2: Subroutine FIND_SLICES adopts information in Zone A and defines the circular arc with coordinates of each slice x, y, x_c, y_c, Δx, and α as graphically illustrated in Zone B of Fig. A.1. The process involves a series of mathematical calculations for the determination of the upper and lower points of interception between the arc and the slope surface, the coordinates defining the slice bases, and so on. Its output serves as feedback to the cells that range between Columns K to Q starting from Row 17 in Zone B. Fig. A.1 depicts the flow chart of this subroutine.

Step 3: Subroutine DATA_UPDATING refreshes the cells in Columns S to AA that stores the information u, h', γ_{avg}, ΔW, c', r_u and ϕ' as defined in Eqs. (1) and (2). They are either directly calculated based on the previously computed data or by functions coded in VBA with the available information stored in Zone A. Fig. A.1 depicts the flow chart of the refreshment. The command 'Subroutine DATA_UPDATING' activates the implementation and refreshes these cells.

Step 4: Subroutine FIND_FOS performs the calculation of Eq. (1). It includes the calculations of the necessary intermediate values and a macro that uses the dynamic programming facility of VBA to find the value of F in Eq. (1) through iterations. The converged solution for the factor of safety is stored in the Cell at Row 15, Column S. The computation details are displayed in worksheet FOS in which the user can check every detail that leads to the factor of safety.

A.3. Searching for the critical slip surface

DBS-IWHR adopts the grid search method to locate the critical slip surface. It consists of two rounds of searches.

The first search varies the x-coordinate of the circle center making a number of trial slip surface all passing the slope toe, as shown in Fig. A.2(a). Usually, a circle associated with the minimum factor of safety F_m can be found, as shown in Fig. A.2 in which $F_m = 0.998$. The relevant information in Fig. A.2(a) can be displayed in worksheet SEARCH 1.
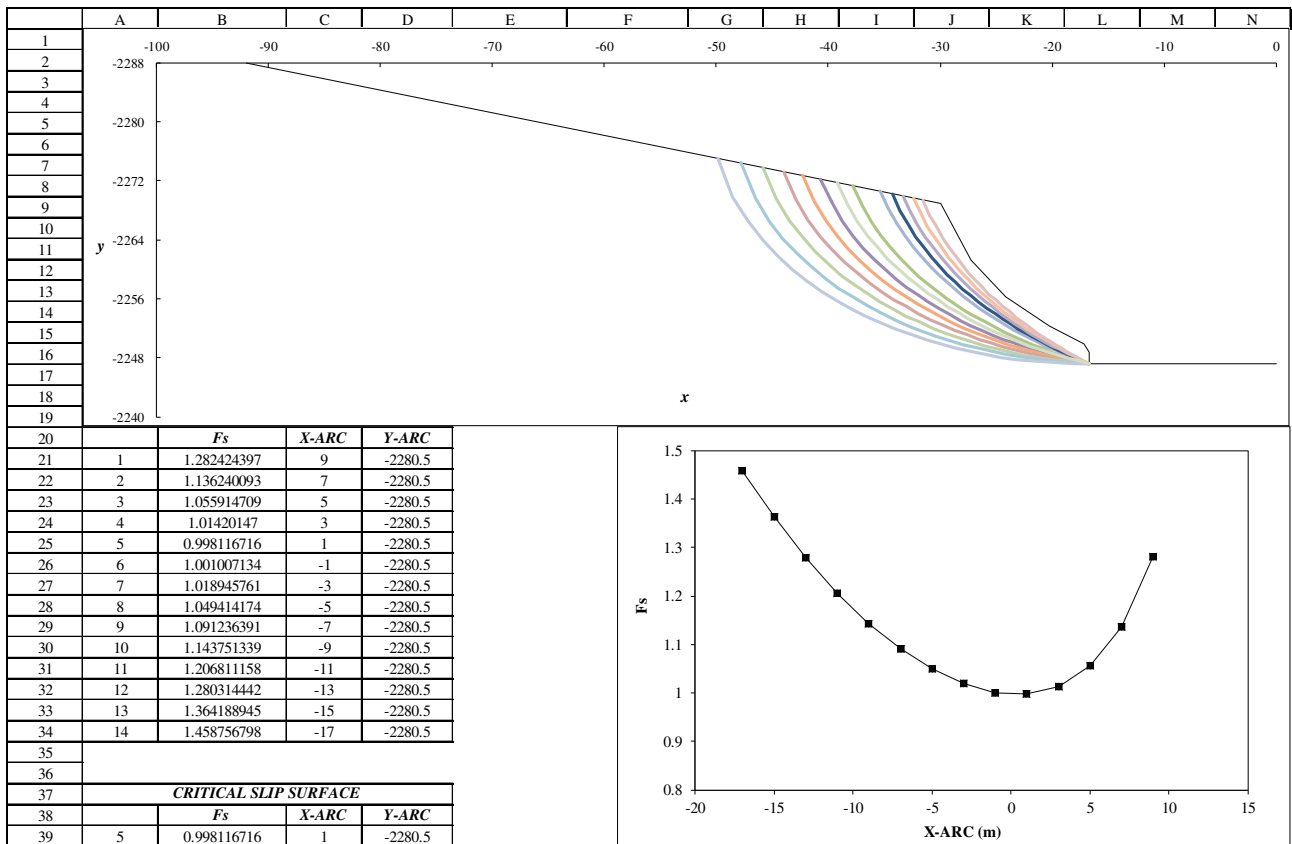

Fig. A.2. Searching for the critical slip surface: (a) the first search; (b) the second search.
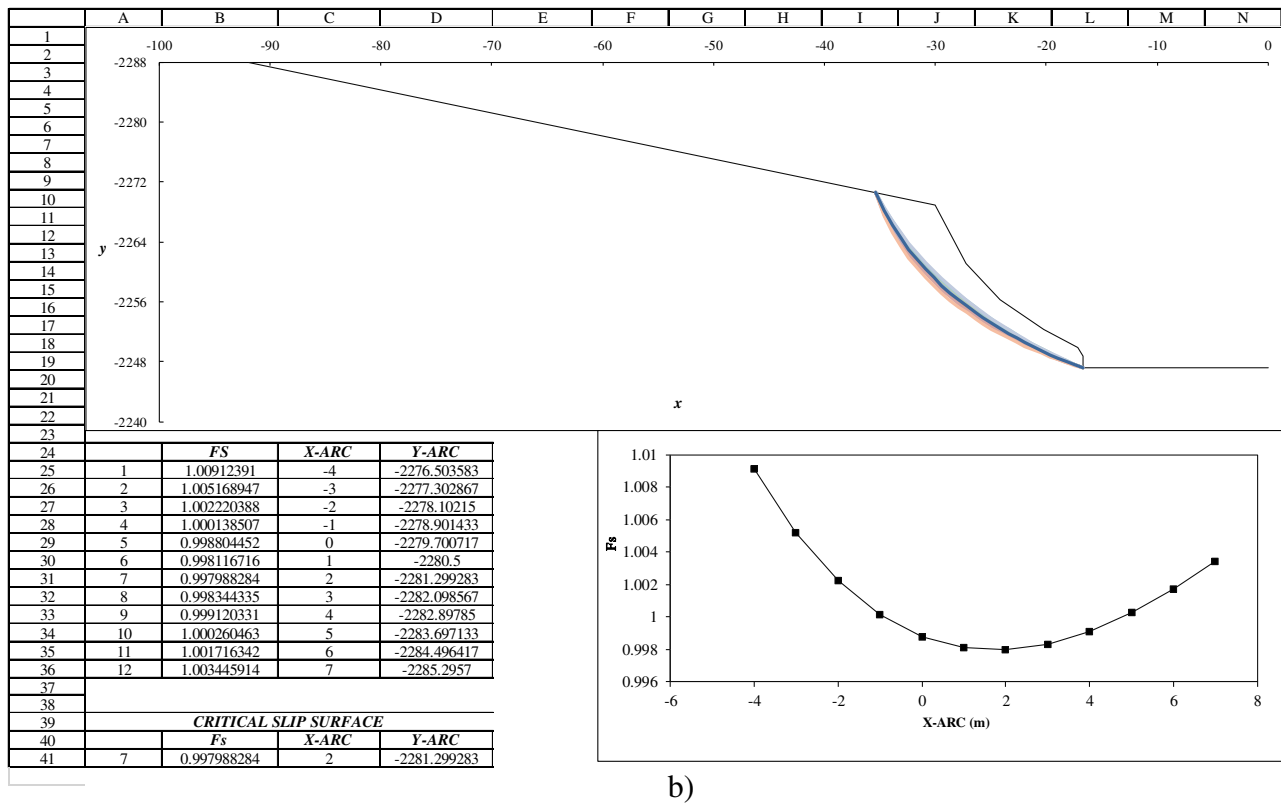
The table and chart embedded in the figure contain the following data:

	FS	X-ARC	Y-ARC
1	1.00912391	-4	-2276.503583
2	1.005168947	-3	-2277.302867
3	1.002220388	-2	-2278.10215
4	1.000138507	-1	-2278.901433
5	0.998804452	0	-2279.700717
6	0.998116716	1	-2280.5
7	0.997988284	2	-2281.299283
8	0.998344335	3	-2282.098567
9	0.999120331	4	-2282.89785
10	1.000260463	5	-2283.697133
11	1.001716342	6	-2284.496417
12	1.003445914	7	-2285.2957

	CRITICAL SLIP SURFACE		
	Fs	X-ARC	Y-ARC
7	0.997988284	2	-2281.299283

b)

Fig. A.2 (continued).

The second search inherits the critical surface obtained in the first step by fixing the upper and lower points of interception and varying the radius of the arc, as shown in Fig. A.2(b). Again, a circle associated with the refined minimum factor of safety can be found. In this example, the refined F_m is 0.997. The relevant information in Fig. A.2(b) can be displayed in worksheet SEARCH 2.

If the first round of search can't find the minimum factor of safety with the required accuracy, a second round of search can then be performed. It follows the same procedure based on the critical slip surface obtained in the first round of search. Since every round of search is just a punch of the keyboard bottom, very little effort is required to find F_m with sufficient accuracy.

References

ASCE/EWRI Task Committee on Dam/Levee Breaching, 2011. Earthen embankment breaching. J. Hydraul. Eng. ASCE 137 (12), 1549–1564.

Bishop, A.W., 1955. The use of the slip circle in the stability analysis of slopes. Géotechnique 5 (1), 7–17.

Bishop, A.W., Morgenstern, N.R., 1960. Stability coefficients for earth slopes. Géotechnique 10 (4), 129–150.

Brown, C.B., 1950. Sediment transportation. In: Rouse, H. (Ed.), Engineering Hydraulics. John Wiley and Sons, New York, pp. 769–857.

Chang, D.S., Zhang, L.M., 2010. Simulation of the erosion process of landslide dams due to overtopping considering variations in soil erodibility along depth. Nat. Hazards Earth Syst. Sci. 10 (4), 933–946.

Chen, Z., Morgenstern, N.R., 1983. Extensions to the generalized method of slices for stability analysis. Can. Geotech. J. 20 (1), 104–119.

Chen, L.H., Chen, Z., Sun, P., 2008. Slope stability analysis using graphic acquisitions and spreadsheets. Proc. 10th Int. Symposium of Landslide and Engineered Slope, Xi'an, Shaanxi, pp. 631–637.

Chen, Z., Ma, L., Yu, S., Chen, S.J., Zhou, X., Sun, P., Li, X., 2015. Back Analysis of the Draining Process of the Tangjiashan Barrier Lake. J. Hydraul. Eng. ASCE 141 (4), 05014011.

D'Eliso, C., 2007. Breaching of sea dikes initiated by wave overtopping: A tiered and modular modeling approach (Ph.D. thesis) Univ. of Braunschweig, Germany, and Univ. of Florence, Italy.

Delaney, K.B., Evans, S.G., 2015. The 2000 Yigong landslide (Tibetan Plateau), rockslide-dammed lake and outburst flood: review, remote sensing analysis, and process modeling. Geomorphology 246, 377–393.

Dou, S.T., Wang, D.W., Yu, M.H., Liang, Y.J., 2014. Numerical modeling of the lateral widening of levee breach by overtopping in a flume with 180° bend. Nat. Hazards Earth Syst. Sci. 14, 11–20.

Duncan, J., 1996. State of the art: limit equilibrium and finite-element analysis of slopes. J. Geotech. Eng. ASCE 122 (7), 577–596.

Einstein, H.A., 1950. The bed-load function for sediment transportation in open-channel flows. Technical Bulletin of the U.S. Dept. of Agriculture Soil Conservation Service, 1026. Washington, DC., USA.

Engelund, F., Hansen, E., 1967. A monograph on sediment transport in alluvial streams. Teknisk Forlag, Copenhagen, Denmark.

Fread, D.L., 1988. BREACH: An erosion model for earthen dam failures (Model description and user manual). National Oceanic and Atmospheric Administration. National Weather Service, Silver Spring, MD, USA.

Huang, J.C., 2008. Numerical modeling of flow through breach of landslide dam. J. Hydraul. Eng. 39 (10), 1235–1240 (in Chinese).

Huang, R.Q., 2012. Mechanisms of large-scale landslides in China. Bull. Eng. Geol. Environ. 71 (1), 161–170.

Johnson, J.J., 1974. Analysis and design relating to embankments. Proc. Conf. on Analysis and Design in Geotechnical Engineering ASCE, New York 2, pp. 1–48.

Liu, N., Chen, Z.Y., Zhang, J.X., Lin, W., Chen, W.Y., Xu, W.J., 2010. Draining the Tangjiashan barrier lake. J. Hydraul. Eng. ASCE 136 (11), 914–923.

Liu, N., Yang, Q.G., Chen, Z.Y., 2015. Hazard mitigation for barrier lakes. Yangtze River Press, Wuhan, China (in Chinese).

Lowe III, J., Karafiath, L., 1960. Stability of earth dams upon drawdown. Proc. First Pan-American Conf. on Soil Mechanics and Foundation Engineering, Mexico City, pp. 537–552.

Low, B.K., Gilbert, R.B., Wright, S.G., 1998. Slope reliability analysis using generalized method of slices. J. Geotech. Geoenviron. Eng. ASCE 124 (4), 350–362.

Lu, J.T., Wang, Z.H., Zhou, C.H., 2003. Discussion on the occurrence of Yigong landslide in Tibet. Earth Sci. J. China Univ. Geosci. 28 (1), 107–110 (in Chinese).

Meyer-Peter, E., Müller, R., 1948. Formulas for bed load transport. Proc. 2nd Meeting of IAHR, Stockholm, Sweden, pp. 39–64.

Mohamed, M.A.A., 2002. Embankment breach formation and modeling methods (Ph.D. thesis) Open University, UK.

Morris, M.W., Kortenhaus, A., Visser, P.J., 2009a. Modeling breach initiation and growth. FLOODsite Rep. T06–08-02, FLOODsite Consortium. (Available from:) www.floodsite.net.

Morris, M.W., Kortenhaus, A., Visser, P.J., Hassan, M.A.A.M., 2009b. Breaching processes: A state of the art review. FLOODsite Rep. T06–06-03, FLOODsite Consortium. Available from: www.floodsite.net.

Morgenstern, N.R., Price, V.E., 1965. The analysis of the stability of general slip surfaces. Géotechnique 15 (1), 79–93.

Osman, A.M., Thorne, C.R., 1988. Riverbank stability analysis. I: Theory. J. Hydraul. Eng. ASCE 114 (2), 134–150.

Peviani, M.A., 1999. Simulation of earth-dams breaking processes by means of a morphological numerical model. CADAM-Concerted Action on Dambreak Modelling: 4th Project Workshop (Zaragoza), Zaragoza, Spain, pp. 381–397.

Peng, M., Zhang, L.M., Chang, D.S., Shi, Z.M., 2014. Engineering risk mitigation measures for the landslide dams induced by the 2008 Wenchuan earthquake. Eng. Geol. 180, 68–84.

Ren, J., Shan, X., Shen, J., Deng, G., Zhang, J., 2001. Geological characteristics and kinematics of the rock-fall landslide in Yi'gong, southeastern Tibet. Geol. Rev. 47 (6), 642–647 (in Chinese).

Shang, Y., Yang, Z., Li, L., Liu, D., Liao, Q., Wang, Y., 2003. A super-large landslide in Tibet in 2000: background, occurrence, disaster, and origin. Geomorphology 54, 225–243.

Sherard, J.L., Woodward, R.J., Gizienski, S.F., Clevenger, W.A., 1963. Earth and Earth-rock Dams. John Wiley and Sons, New York, USA.

Singh, V.P., Scarlatos, P.D., 1988. Analysis of gradual earth-dam failure. J. Hydraul. Eng. ASCE 114 (1), 21–42.

Skempton, A.W., 1954. The pore-pressure coefficient A and B. Géotechnique 4 (4), 143–147.

U.S. Army Corps of Engineers, 1970. Engineering and design, stability of earth and rock-fill dams: Engineer manual. Dept. of the Army, Corps of Engineers, Washington, DC.

Viero, D.P., D'Alpaos, A., Carniello, L., Defina, A., 2013. Mathematical modeling of flooding due to river bank failure. Adv. Water Resour. 59, 82–94.

Wang, G.Q., Liu, F., Fu, X.D., Li, T.J., 2008. Simulation of dam breach development for emergency treatment of the Tangjiashan Quake Lake in China. Sci. China Ser. E: Technol. Sci. 51 (2), 82–94.

Wen, B., Wang, S., Wang, E., Zhang, J., 2004. Characteristics of rapid giant landslides in China. Landslides 1 (4), 247–261.

Wu, W., 2013. Simplified physically based model of earthen embankment breaching. J. Hydraul. Eng. ASCE 139 (8), 837–851.

Xu, Q., Shang, Y., van Asch, T., Wang, S., Zhang, Z., Dong, W., 2012. Observations from the large, rapid Yigong rock slide-debris avalanche, southeast Tibet. Can. Geotech. J. 49 (5), 589–606.

Yin, Y.P., 2000. Characteristics of Bomi– Yigong huge high speed landslide in Tibet and the research on disaster prevention. Hydrogeol. Eng. Geol. 4, 8–11 (in Chinese).

Yin, Y., Xing, A., 2012. Aerodynamic modeling of the Yigong gigantic rock slide-debris avalanche, Tibet. China. Bull. Eng. Geol. Environ. 71 (1), 149–160.

Zhang, J.Y., Lu, Y., Xuan, G.X., Wang, X.G., Li, Y., 2009. Overtopping breaching of cohesive homogeneous earth dam with different cohesive strength. Sci. China E: Technol. Sci. 52 (10), 3024–3029.

Zhang, M., Yin, Y.P., 2013. Dynamics, mobility-controlling factors and transport mechanisms of rapid long-runout rock avalanches in China. Eng. Geol. 167, 37–58.

Zhou, J.W., Cui, P., Hao, M.H., 2015. Comprehensive analyses of the initiation and entrainment processes of the 2000 Yigong catastrophic landslide in Tibet, China. Landslides 13 (1), 39–54.

Zhu, P.Y., Wang, C.H., Wang, Y.C., 2003. Large-scale landslide-debris avalanche in Tibet, China. Formation of an exceptionally serious outburst flood from a landslide dam in Tibet. Landslide News 14-15, 23–25.

Zhu, Y.H., 2006. Breach growth in clay-dikes (Ph.D. thesis) Delft University of Technology, Delft, the Netherlands.